JOURNAL OF PROPULSION AND POWER
Vol. 26, No. 6, November–December 2010

Acoustic Characterization of an Ethylene-Fueled Scramjet Combustor with a Cavity Flameholder

Kuo-Cheng Lin*
Taitech, Inc., Beavercreek, Ohio 45430
Kevin Jackson,† Robert Behdadnia,‡ and Thomas A. Jackson§
U.S. Air Force Research Laboratory, Wright-Patterson Air Force Base, Ohio 45433
and
Fuhua Ma¶ and Vigor Yang**
Pennsylvania State University, University Park, Pennsylvania 16802

DOI: 10.2514/1.43338

Past experience with ramjet engines suggests that combustion instabilities and associated flow oscillations may also occur in scramjet engines, although the problem has not been recognized and explored yet. The present work investigated thermoacoustic instabilities inside an ethylene-fueled scramjet combustor with a recessed-cavity flameholder. Detailed characterization was made of flame oscillation and acoustic motion using high-speed photography and pressure measurements. The effects of fuel/air equivalence ratio, fueling scheme, and simulated flight conditions on the stability characteristics in the engine flowpath were examined systematically. In addition, an analytical analysis based on the acoustic and convective feedback loops among the precombustion shock, fuel injection, and distributed flame was established to help understand and correlate the observed oscillation phenomena. The oscillation frequencies fall in a range of 100–400 Hz, with the upper bound dictated by the shock–flame coupling mechanism and the lower bound by the injector–flame interaction.

Nomenclature

A_d	=	acoustic admittance function
a	=	speed of sound
ER	=	fuel equivalence ratio
$\mathrm{ER}_{\mathrm{body}}$	=	fuel equivalence ratio from body wall
f	=	frequency
h_c	=	heat of combustion per unit mass of fuel
L	=	characteristic length
M	=	Mach number
$\dot{m}$	=	mass flow rate of fuel/air mixture
$\dot{m}_{\mathrm{air}}$	=	mass flow rate of vitiated air
$\dot{m}_f$	=	mass flow rate of fuel
M_{flight}	=	simulated flight Mach number
M_{nozzle}	=	facility nozzle Mach number
p	=	pressure
$\dot{Q}$	=	overall heat-release rate
q	=	dynamic pressure or specific heat release
T	=	temperature
u	=	convective velocity in freestream direction
x_i	=	injector location
x_f	=	peak temperature location
x_s	=	shock train leading-edge location
β	=	acoustics reflection coefficient
γ	=	specific heat ratio
τ	=	characteristic time
ϕ	=	equivalence ratio
Ω	=	dimensionless frequency
$\bar{(\,)}$	=	time-averaged values
$\underline{(\,)}$	=	spatial-averaged values

Subscripts

if	=	feedback loop between injection site and flame zone
$sf1$	=	acoustic feedback loop between shock train and flame zone
$sf2$	=	acoustic-convective feedback loop between shock train and flame zone
0	=	stagnation condition

Superscript

$'$	=	temporal fluctuations

Presented as Paper 2007-5382 at the 43rd AIAA/ASME/SAE/ASEE Joint Propulsion Conference & Exhibit, Cincinnati, OH, 8–11 July 2007; received 20 January 2009; revision received 28 April 2010; accepted for publication 12 May 2010.

*Senior Research Scientist, 1430 Oak Court, Suite 301; Kuo-Cheng.Lin@wpafb.af.mil. Associate Fellow AIAA (Corresponding Author).
†Aerospace Engineer, AFRL/RZAS. Member AIAA.
‡Program Manager, AFRL/RZAS.
§Division Chief, AFRL/RZA. Associate Fellow AIAA.
¶Postdoctoral Research Associate, Department of Mechanical Engineering. Member AIAA.
**John L. and Genevieve H. McCain Chair in Engineering, Department of Mechanical and Nuclear Engineering; currently Georgia Institute of Technology; vigor.yang@aerospace.gatech.edu. Fellow AIAA.

I. Introduction

COMBUSTION-INDUCED oscillations (commonly known as combustion instabilities) have plagued the development of a wide spectrum of rocket [1–3] and airbreathing [4] propulsion systems. The root cause is the interaction between transient combustion response and unsteady flow motion in a confined volume in which acoustic waves can be easily excited and sustained. Only an exceedingly small fraction of the chemical energy released in the combustion process is required to generate large excursions of acoustic oscillations. The resultant vibration and excessive heat transfer often lead to a severe damage to the system.

Past experience with the development of ramjet engines [5] suggests that combustion instability may also occur in scramjet engines, although the problem has not been recognized and explored to a large extent yet. One common assumption is that because acoustic waves

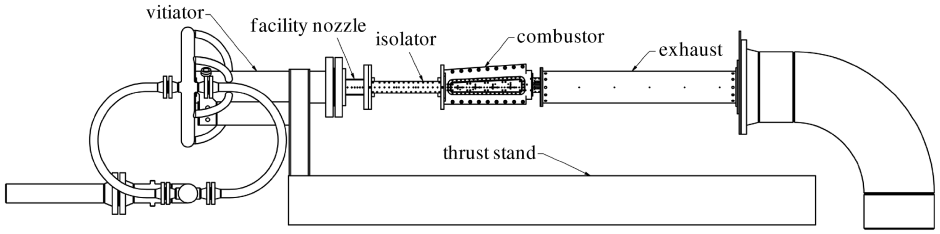

Fig. 1 Schematic of supersonic combustion facility.

cannot propagate upstream in a supersonic-flow environment, any flow oscillations arising in the flame zone will simply travel downstream and exit from the engine without forming the feedback loop required for sustaining combustion and flow instabilities. In reality, this picture may not be correct. Acoustic waves can propagate upstream in various subsonic-flow regions in a scramjet engine, such as boundary layers and recirculation zones in the flame-holding cavity. Furthermore, fuel injection in a supersonic cross flow and the associated shock-wave/boundary-layer interactions are intrinsically unsteady. The numerical analysis by Choi et al. [6] for a hydrogen-fueled scramjet has clearly demonstrated such flow instability. The resultant oscillation may interfere with engine operation severely. Recent experiments in hydrocarbon fueling for scramjet engines have also revealed the presence of flow oscillations with frequencies of 90–120 Hz for liquid JP-7 fuel and 300–360 Hz for gaseous ethylene fuel [7]. The dominant frequency increases as the equivalence ratio decreases, a phenomenon that can be attributed to the mutual coupling between the fuel injection/mixing process and unsteady heat release in the flame zone. The oscillation frequency is dictated by the time required for an acoustic wave to propagate upstream from the combustion zone to the fuel injection location and the time for the mixture fluctuation to travel downstream to the flame front. At a higher equivalence ratio, the flame spreads further downstream in the chamber, rendering a lower oscillation frequency.

The present work investigates, both experimentally and analytically, thermoacoustic instabilities inside an ethylene-fueled supersonic combustor with a cavity flameholder. High-speed pressure transducers, positioned at the base and downstream of the cavity flameholder, are used to record acoustic signals over a wide range of operating conditions. The effects of fuel/air equivalence ratio, fueling scheme, cavity length, and simulated flight conditions on the stability characteristics of the combustor are examined systematically. The measured flow oscillation frequencies and the corresponding amplitudes are used to explore the underlying flow physics. In addition, the measurements are compared with existing acoustic data for different combustor flowpaths to help identify the mechanisms responsible for driving and sustaining combustion oscillations. An analytical model based on the acoustic/convective feedback loops between the shock and flame and on the acoustic-convective feedback loop between the fuel injector and flame is developed to help understand and correlate the observed oscillation phenomena.

II. Experimental Methods

Experiments were carried out on the thrust stand inside Test Cell 18 at Wright-Patterson Air Force Base. This facility was designed for fundamental studies of supersonic reacting flows using a continuous-run, open-loop air flow supply with a direct-connect configuration. The entire test rig consists of a natural-gas fueled vitiator, an interchangeable facility nozzle (Mach 1.8 or 2.2), a modular isolator, a modular combustor, and an exhaust pipe, as illustrated in Fig. 1. The rig is mounted to a thrust stand capable of measuring thrust of up to 2000 lbf (8896 N). A series of compressors are employed to provide air up to 30 lb/s (13.6 kg/s), with a total pressure and temperature up to 750 psia (51.0 atm) and 1600 R (889 K), respectively. An exhaust system is used to lower the pressure to 3.5 psia (0.238 atm) and to maintain backpressure for smooth starting and safe operation. Combined with the supersonic facility nozzle, the air vitiator can be modulated to simulate flight Mach numbers of 3.5–5.0 with dynamic pressures of 500–2000 psf (0.236–0.943 atm). Table 1 lists the flight conditions of interest in the present study and the corresponding vitiator operating conditions. The low flight Mach numbers correspond to the scramjet takeover phase, during which the flow transients, ignition, and flame development take place. Under these conditions, the combustor operates in a dual-mode fashion, that is, the combustion takes place at both subsonic and supersonic region [8,9].

The scramjet flowpath consists of a heat-sink rectangular isolator and a rectangular combustor featuring a recessed-cavity flameholder and flush-mounted, low-angled injectors, as shown in Fig. 2. A high-resolution pressure transducer was installed downstream of the flameholder on the body wall. The isolator has a rectangular cross-sectional area with a height of 1.5 in. (38.1 mm), a width of 4.0 in. (101.6 mm), and a length of 25.75 in. (654.0 mm). The interior surface of the isolator was coated with a layer of 0.02-in.-thick (0.51-mm-thick) thermal barrier coating to protect the metal wall from excessive heating by the vitiated hot air during long tests. The combustor measures 36 in. (914.4 mm) in length and has a constant divergence angle of 2.6 deg. The interior surface of the combustor is covered with either heat-sink or water-cooling panels, depending on the anticipated heat load at particular locations. All of these panels were coated with thermal barrier coating for additional thermal protection. Two water-cooled combustor side-wall inserts can be

Table 1 Simulated flight conditions

M_{flight}	M_{nozzle}	q, psf (kPa)	T_0, R (K)	p_0, psia (atm)	$\dot{m}_{\text{air}}$, lb/s (kg/s)
5.0	2.2	2000 (95.8)	1913 (1063)	208.3 (14.2)	6.87 (3.12)
5.0	2.2	1000 (47.9)	1950 (1083)	103.0 (7.01)	3.36 (1.52)
5.0	2.2	500 (23.9)	1992 (1107)	51.60 (3.51)	1.67 (0.757)
4.5	2.2	2000 (95.8)	1766 (981.1)	211.2 (14.4)	7.25 (3.29)
4.5	2.2	1000 (47.9)	1792 (995.6)	103.5 (7.04)	3.53 (1.60)
4.5	2.2	500 (23.9)	1828 (1016)	51.40 (3.50)	1.74 (0.789)
4.0	1.8	2000 (95.8)	1389 (771.7)	102.3 (6.96)	5.75 (2.61)
4.0	1.8	1000 (47.9)	1398 (776.7)	53.50 (3.64)	3.00 (1.36)
4.0	1.8	500 (23.9)	1424 (791.1)	26.40 (1.80)	1.47 (0.667)
3.5	1.8	2000 (95.8)	1253 (696.1)	106.9 (7.27)	6.33 (2.87)
3.5	1.8	1000 (47.9)	1253 (696.1)	52.10 (3.55)	3.09 (1.40)
3.5	1.8	500 (23.9)	1278 (710.0)	25.70 (1.75)	1.50 (0.680)

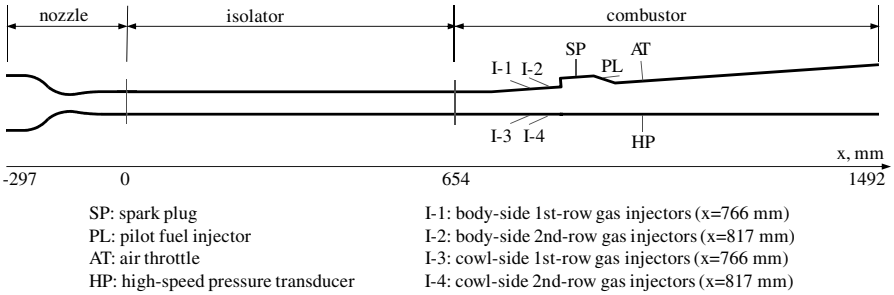

Fig. 2 Schematic of combustor flowpath and key interior features.

replaced with quartz windows for flame visualization and optical measurements.

A recessed-cavity flameholder is located on the divergent top wall, which is designated as the body side of a scramjet-powered vehicle. Figure 3 shows the integrated injection unit, cavity flameholder, and air throttling block on the vehicle body wall. The cavity spans the entire flowpath width and has a forward-facing ramp to effectively interact with the shear layer originating from the cavity leading edge [8]. This cavity was scaled down from the design employed in the study of Mathur et al. [10], which considered a slightly larger scramjet flowpath. The flame-holding cavity is 0.675 in. (1.67 cm) deep, with a base of 2.57 in. (6.5 cm) length, and a closeout ramp of 22.5 deg. The leading edge of the cavity is located 5.4 in. (13.7 cm) downstream of the combustor entrance. Two spark plugs located at the base of the cavity were used as the baseline ignition source.

Four banks of gaseous fuel injectors, two on the top (body) and two on the bottom (cowl) walls, were implemented to provide various fueling options, as shown in Fig. 2. The sites were selected so that the effects on the ignition and combustion characteristics of the injection location and fueling split between the body and cowl walls can be evaluated. Body-side-only fueling from I-1 or I-2 injectors and a 60/40 fueling split between the body- and cowl-side injectors (for example, I-2/I-4 at 60/40) were chosen as the baseline fueling schemes. There are 4 orifices on each body-side injection site and 3 orifices on each cowl-side injection site. Each fuel injector features a flush-wall plain orifice with a 15 deg angle from the downstream wall plane. Each hole is 0.125 in. (0.318 cm) in diameter. The upstream (I-1 and I-3) and downstream (I-2 and I-4) fuel injectors are located around 1.4 in. (3.6 cm) and 3.4 in. (8.6 cm) downstream of the combustor entrance, respectively.

Pressure taps and thermocouple ports were positioned throughout the entire rig for instrumentation and condition monitoring. The data acquisition system consists of a crate based on computer-automated measurement and control (128 analog inputs, 16 analog outputs, 48 digital inputs and 32 digital outputs channels), a 256-channel electronic pressure scanning system (Pressure Systems, Inc.), and a 64-channel thermocouple scanning system (Scanivalve Corporation). The flow rates of vitiated air, makeup oxygen, ethylene, and throttling air were measured using orifice plates, sonic nozzles, Venturi flow meters, and turbine flow meters. Instrumentation readings were recorded directly or with preliminary reductions into a Linux-based PC at 2–10 Hz frequency via fiber optic and Ethernet cable. A high-frequency pressure transducer (100 mV/psi sensitivity, model 112A22, PCB Group, Inc.) with a signal conditioner (model 482A20, PCB Group, Inc.) was used to identify the acoustic characteristics in the combustor. The transducer was located at the center span on the cowl wall and was 15.5 in. (394 mm) from the combustor entrance.

The testing sequence for each run started with creating the desired vitiator operating condition. Once the vitiator pressure and temperature were on condition, unheated ethylene was then injected according to the selected fueling scheme. Ignition was first attempted with spark plugs only. If no ignition was achieved, air throttling was activated for about 1–3 s to create a favorable environment for ignition and flame stabilization [11]. The air throttling ports were located downstream of the cavity flame holder on the body wall, as indicated in Fig. 3. The flame-on duration lasted about 20–40 s with a constant fuel flow rate until the temperatures at high heat-load locations approached the preset limits. Spark plugs were on during the entire flame-on duration, even though attempts to turn off the spark plug after the ignition did not extinguish the flame.

III. Results and Discussion

A. Flame Visualization

Experiments were conducted to study the flame characteristics in the scramjet combustor under various simulated flight conditions. Figure 4 shows snapshot of the flame configuration at dynamic pressures of 1000 psf and flight Mach number of 5.0. Gaseous ethylene is injected from the I-2 ports, and the overall equivalence ratio is 1.04. The flow is from the left to the right. The flame is anchored by the recirculating flow in the cavity and spreads downstream from the corner of the rear-facing step. It also propagates a short distance along the boundary layer on the body wall slightly upstream of the cavity. In addition, observations were made of the flame propagation along the combustor sidewalls. Figure 5 shows the flame evolution inside the scramjet combustor. The flame is intrinsically unsteady and oscillates periodically in response to the acoustic-flow motions in the combustor. This phenomenon will be

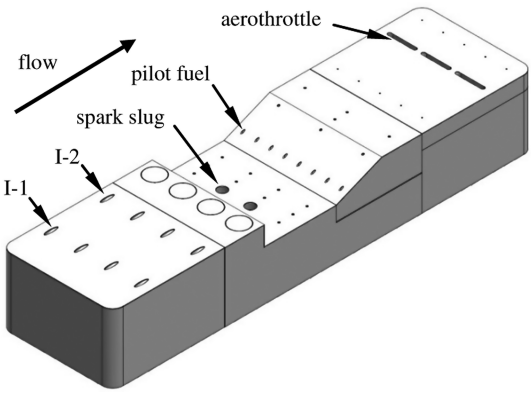

Fig. 3 Integrated fuel injector, cavity flameholder, and aerothrottle.

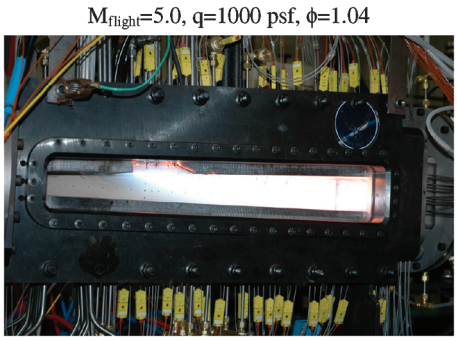

Fig. 4 Photographs of flame inside scramjet combustor; $M_{flight} = 5.0$, $q = 1000$ psf, and $\phi = 1.04$; unheated ethylene was injected from the I-2 injection site.

Fig. 5 Flame evolution inside scramjet combustor showing oscillation; $M_{\text{flight}} = 5.0$ and $q = 1000$ psf.

considered later. No images with other fueling schemes were taken, due to the failure of the quartz window from excessive thermal shock.

B. Effect of Fueling Distribution

The effect of fuel distribution on combustion characteristics was explored over a wide range of equivalence ratios. Figure 6 shows the wall static pressure profiles. The simulated flight Mach number was between 3.5 to 5.0 for two different dynamic pressures of $q = 500$ and 1000 psf. The baseline injection site is I-2, whose fuel plumes can closely interact with the cavity flameholder for the establishment of sustained combustion. The fueling schemes include: 1) I-2 only, 2) combined I-2/I-3, and 3) combined I-2/I-4 injection. Cowl-side fueling is expected to consume the unburned freestream air, which may not be reached by the body-side flame. For the present study, a fueling split with a 60/40 ratio between the body- and cowl-side injectors was selected for the (I-2/I-3) and (I-2/I-4) injection schemes. Delivering more fuel from the cowl-side injectors was expected to be ineffective, mainly due to the lack of flame-holding mechanisms to facilitate the cowl-side combustion within the given length of the present flowpath, as will be illustrated later. The flight conditions in Figs. 6a and 6b were simulated with the Mach 1.8 facility nozzle for the flight Mach numbers of 3.5 and 4.0, respectively. The Mach 2.2 nozzle was used to simulate the flight conditions in Figs. 6c and 6d, which correspond to flight Mach numbers of 4.5 and 5.0, respectively. Test conditions with an almost identical overall fuel equivalence ratio are also included in Fig. 6 for comparison.

For the cases with relatively low flight Mach numbers in Figs. 6a and 6b, with the same equivalence ratio, a 60/40 fuel split between the body- and cowl-side injectors leads to a lower pressure rise in the combustor, as compared with body-side-only injection. See Figs. 6a and 6b for runs F06164AJ vs F06164AW and F06164AP for $M_{\text{flight}} = 3.5$ and runs F06165AI vs F06165AH for $M_{\text{flight}} = 4.0$. Apparently, the fuel withdrawn from the body side and distributed to the cowl side of the combustor does not contribute to efficient combustion for either flight condition. With a smaller amount of fuel to directly interact with the flame ignition source and the cavity flameholder, the resulting flame spreading stays close to the body wall. Flame spreading toward the cowl wall to ignite the cowl-side fuel plumes at both simulated flight conditions is, therefore, limited within the given combustor length. As a result, the injected cowl-side fuel might not combust without the additional set of flameholder and ignition source on the cowl wall. This observation highlights the importance of a flame-holding device to facilitate flame ignition and flame stabilization inside a hydrocarbon-fueled scramjet flowpath at low flight Mach numbers.

On the other hand, the same fuel split attains higher pressure rises for the simulated flight Mach numbers of 4.5 and 5.0, as shown in Figs. 6c and 6d. Unlike the observations in Figs. 6a and 6b, the redistributed fuel on the cowl wall actually brings additional benefit to the combustor operation for higher flight Mach numbers. One possible explanation for the observed difference between high and low flight Mach numbers regarding the effects of fuel split might come from the difference in the reactivity of fuel/air mixtures. With a higher total temperature inside the vitiator to simulate high Mach number condition, as can be seen in Table 1, the reactivity of the fuel/air mixtures increases [8]. Therefore, the absence of the cowl-side cavity flameholder appears to be less vital for the combustion of the cowl-side fuel, as long as the flame spreading from the body wall is sufficient to reach the cowl-side fuel plumes or the local temperature and pressure facilitate autoignition of the cowl-side fuel/air mixtures. It should be noted that the improved pressure rises with the present 60/40 fuel split at high flight Mach number conditions may not apply to a flowpath with a duct height, where the body-side flame may not reach the cowl-side fuel plumes, or a convergence angle larger than the present configuration, where the expansion process may prohibit the autoignition of the cowl-side fuel/air mixtures. Further analyses or testing should be carried out to find out the effects of cowl-side fueling in different flowpaths. Nonetheless, one may conclude that cowl-side fueling can be beneficial to the performance of a rectangular scramjet combustor with a body-side flameholder if proper flame spreading and favorable reactivity of local fuel/air mixtures can be established.

While the I-1 and I-2 injection schemes (not shown) produce significantly different shock train locations and pressure rises in the chamber, no significant difference was observed between the (I-2/I-3) and (I-2/I-4) fueling schemes at the same overall fuel equivalence ratio. The relatively small sensitivity to the choice of the I-3 or I-4 injection site for those fuel split cases indicates that the additional fuel penetration from the I-3 injection site is not sufficient to make advantageous coupling with the body-side flame.

C. Acoustic Measurements

Combustion oscillations and associated flow instabilities have been a concern in the development of scramjet engines. For hydrogen-fueled systems, autoignition may occur in a supersonic stream as long as the local flow temperature and pressure, as well as the mixture stoichiometry, fulfill the condition for sustained reactions [8]. The situation with hydrocarbon fuels, however, is considerably different. The flame can seldom be ignited in a supersonic stream due to the relatively long time required for ignition, compared with the quite short flow residence time. The flame must be anchored in a low-speed subsonic region and spreads gradually into the downstream supersonic region. The induced flow oscillations then either travel downstream in the form of convective and acoustic waves, or propagate upstream in the form of acoustic waves through various subsonic regions in the flowpath (notably, wall boundary layers,

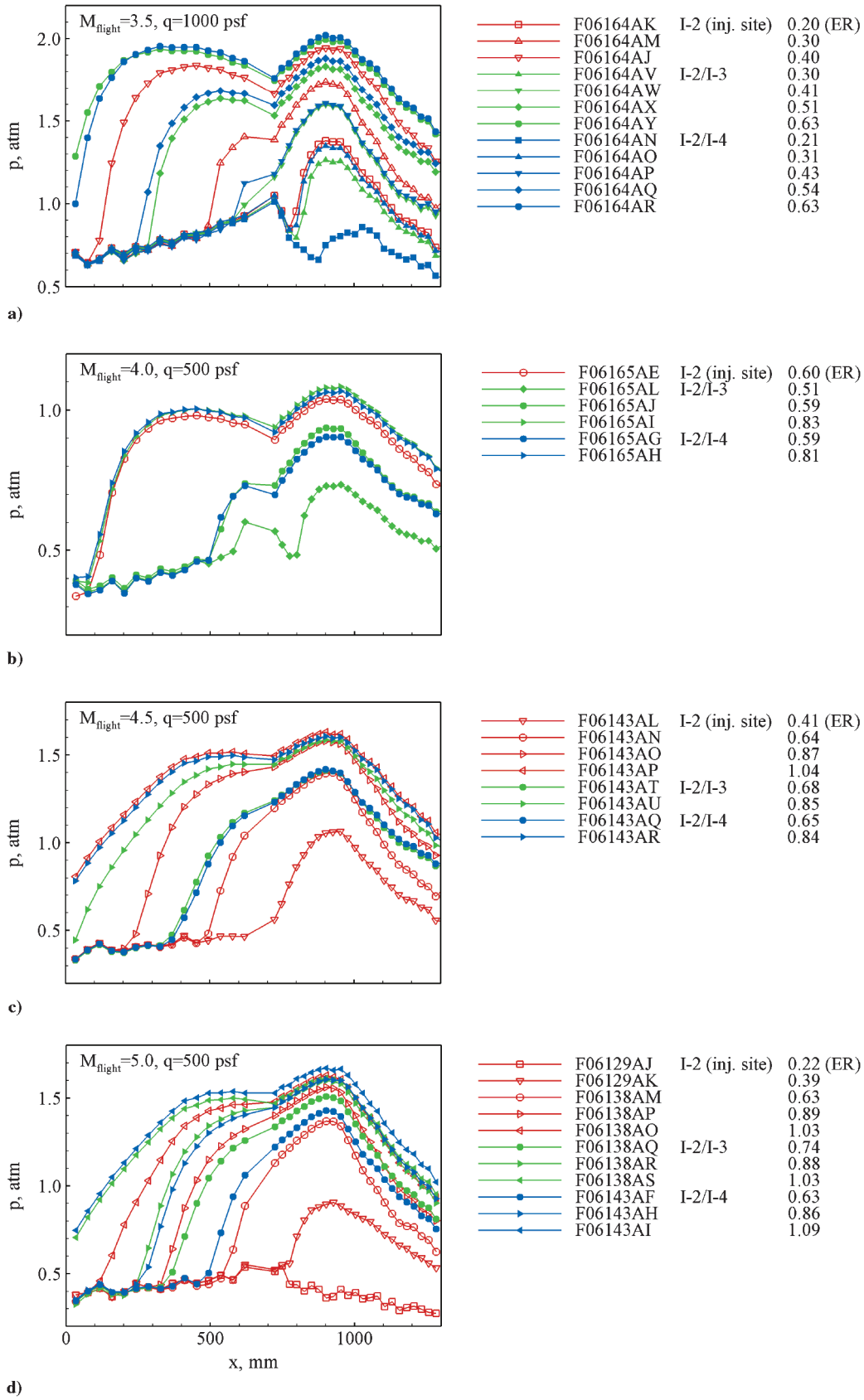

Fig. 6 Distributions of wall static pressures for three different fueling schemes with various fuel equivalence ratios: a) $M_{\text{flight}} = 3.5$ and $q = 1000$ psf, b) $M_{\text{flight}} = 4.0$ and $q = 500$ psf, c) $M_{\text{flight}} = 4.5$ and $q = 500$ psf, and d) $M_{\text{flight}} = 5.0$ and $q = 500$ psf; $x = 0$ marks the isolator entrance.

corner recirculation zones, and the subsonic region behind the precombustion shock train). The upstream-running acoustic wave gives rise to oscillations in the fuel injection/mixing process and shock motion, which subsequently affects the combustion process. A feedback loop is thus formed for driving and sustaining flow oscillations in the engine. The flame may be extinguished if the oscillation amplitude exceeds the limit for the flame stability. Recent experiments with a similar flowpath have demonstrated pressure

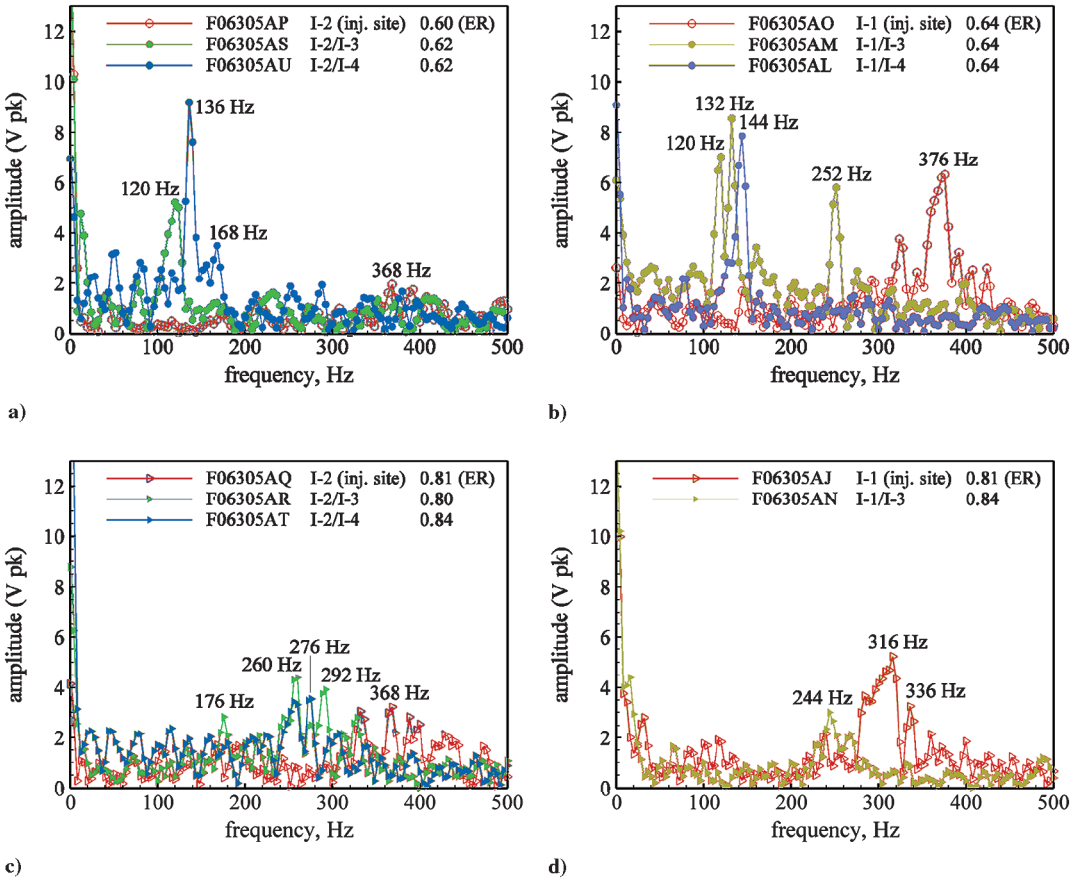

Fig. 7 Frequency spectra of pressure oscillations for various fueling schemes and equivalence ratios; ethylene fuel with $M_{\text{flight}} = 4.5$ and $q = 500$ psf.

oscillations with dominant frequencies of 90–120 Hz for liquid JP-7 fuel and 300–360 Hz for ethylene fuel [7]. The feedback loop between the fuel injection and the heat release zone was identified as the main driving mechanism for the observed pressure oscillations. To provide deeper insight into this phenomenon and to acquire a more complete data base, more detailed pressure measurements were made in the present study using various fueling schemes.

Figure 7 shows the frequency spectra of measured pressure oscillations downstream of the cavity (see Fig. 2) for several different fuel-injection schemes. The simulated flight Mach number and dynamic pressure were fixed at 4.5 and 500 psf (0.236 atm). For an equivalence ratio of 0.60, as shown in Fig. 7a, a dominant frequency of 368 Hz was observed for the I-2 only fueling scheme. Low-frequency oscillations then occurred in the range of 120–140 Hz when a 60/40 fuel split was introduced.

The shift in oscillation frequency was also observed for injection schemes using the I-1 site, as shown in Fig. 7b. As the cowl-side injection was introduced, the dominant frequency shifted from 376 Hz for the I-1 only injection to 120–140 Hz for the case with 60/40 fuel split. With the I-1 only injection, the amplitude of the dominant pressure oscillation is significantly higher than with the I-2 only injection scheme, even at a similar equivalence ratio. In addition, a second pressure oscillation with a frequency of 252 Hz prevailed for the (I-1/I-3) injection scheme.

As the equivalence ratio increased from 0.6 to 0.8, the low-frequency oscillations of 120–140 Hz for the injection schemes with 60/40 fuel split became insignificant. Instead, oscillations with frequencies in the range of 240–290 Hz emerged. The oscillation characteristics associated with the body-side-only injection remained unchanged, even with an increase in the equivalence ratio. In general, the I-2 only injection scheme resulted in relatively stable combustion for all the conditions considered in Fig. 7. The I-1 only injection site led to a higher-amplitude oscillation of 316 Hz, as evidenced in Fig. 7d.

D. Oscillation Mechanisms

To understand the underlying mechanisms for the observed flow oscillations, we considered various feedback loops in the subsonic region bounded by the precombustion shock in the isolator and the thermal throat in the downstream region of the flame zone. No such acoustic feedback may exist in a supersonic regime. Three different mechanisms were identified, involving the coupling of the flame zone with the precombustion shock and fuel injection, respectively, as illustrated in Fig. 8.

The first and second mechanisms are concerned with the coupling between the terminal shock and flame zone. As a consequence of unsteady heat release, acoustic waves are produced in the combustor and propagate upstream to interact with the shock wave in the isolator. The resultant flow oscillations in the isolator either propagate downstream in the form of acoustic waves, or are convected downstream with the local flow velocity in the form of vorticity and entropy waves, which then reinforce the unsteady motions in the flame zone. The response of a normal shock to downstream disturbances can be conveniently characterized using an acoustic admittance function [12–14], expressed as follows:

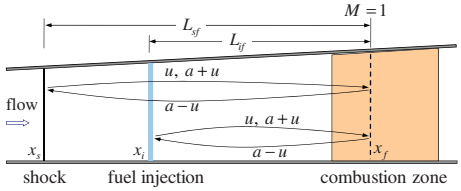

Fig. 8 Acoustic-convective feedback loops and associated characteristic velocities in a scramjet combustor (first: shock–flame acoustic feedback, second: shock–flame acoustic-convective feedback, and third: injector–flame feedback).

$$A_d \equiv \frac{u'/\bar{a}_2}{p'/\gamma\bar{p}_2} = \frac{-\frac{2}{\gamma+1}\cdot\frac{\bar{M}_1^2+1}{\bar{M}_1^2}\Omega i + \frac{2\gamma\bar{M}_2}{\gamma+1}}{\frac{4\bar{M}_1}{\gamma+1}\left(\frac{\bar{p}_1}{\bar{p}_2}\frac{\bar{a}_2}{\bar{a}_1}\right)\Omega i - \frac{\gamma^2+1}{\gamma^2+\gamma}\cdot\left(\bar{M}_1^2+\frac{\gamma-1}{\gamma^2+1}\right)\left(\bar{M}_1^2-\frac{\gamma-1}{2\gamma}\right)^{-1}} \tag{1}$$

where $\bar{p}$, $\bar{a}$, and $\bar{M}$ are the mean pressure, speed of sound, and Mach number, respectively, and γ is the specific heat ratio. The subscripts 1 and 2 stand for the quantities immediately upstream and downstream of the shock, respectively. The admittance function A_d is a complex variable. The dimensionless frequency Ω is defined as

$$\Omega = \frac{2\pi f}{\bar{a}_2}\left(\frac{1}{A}\frac{\mathrm{d}A}{\mathrm{d}x}\right)_s^{-1} \tag{2}$$

where f is the oscillation frequency, A denotes the cross-sectional area, and subscript s represents the value at the terminal shock. The acoustic reflection coefficient is related to the admittance function as

$$\beta = \frac{1+A_d}{1-A_d} \tag{3}$$

The above analysis was established based on the assumption of inviscid flow. The shock acts as an effective acoustic damper absorbing disturbances arising from the downstream region [12–15]. In reality, the acoustic reflection coefficient of a shock may reach a considerable value due to the presence of boundary layers and their interactions with the shock wave. Furthermore, strong vortical waves may be generated by the oscillating shock in the boundary layers. Shock-induced entropy waves and airflow fluctuation may also occur [13,14]. Purely acoustic and acoustic-convective feedback loops between the shock and flame zone are thus established, with characteristic times that can be estimated, respectively, as

$$\tau_{sf1} = \int_{x_s}^{x_f}\frac{\mathrm{d}x}{a-u} + \int_{x_s}^{x_f}\frac{\mathrm{d}x}{a+u} \approx \frac{L_{sf}}{\underline{a}-\underline{u}} + \frac{L_{sf}}{\underline{a}+\underline{u}} = \frac{2L_{sf}}{\underline{a}(1-\underline{M}^2)} \tag{4}$$

$$\tau_{sf2} = \int_{x_s}^{x_f}\frac{\mathrm{d}x}{a-u} + \int_{x_s}^{x_f}\frac{\mathrm{d}x}{u} \approx \frac{L_{sf}}{\underline{a}-\underline{u}} + \frac{L_{sf}}{\underline{u}} = \frac{L_{sf}}{\underline{a}\,\underline{M}(1-\underline{M})} \tag{5}$$

where $\underline{a}$ and $\underline{M}$ represent the speed of sound and Mach number longitudinally averaged between the shock and flame, respectively, and x_s and x_f are the locations of the shock and flame, respectively. The corresponding oscillation frequencies f_{sf1} and f_{sf2} are

$$f_{sf1} = 1/\tau_{sf1}; \qquad f_{sf2} = 1/\tau_{sf2} \tag{6}$$

The third mechanism deals with the region between the fuel injection and flame zone. The acoustic wave generated in the flame zone propagates upstream and causes an air mass flow-rate oscillation in the fuel injection/mixing region. If the fuel injection rate is fixed (e.g., through a choked nozzle), the fuel/air mixture ratio then fluctuates according to the local air flow rate. The resultant oscillation is convected downstream to modify the stoichiometry in the flame zone [12]. The ensuing fluctuation in the overall heat-release rate $\dot{Q}$ can be determined by the fuel consumption rate $\dot{m}_f$. For longitudinal oscillations in a quasi-one-dimensional flow, the specific heat-release q can be written as

$$q = \dot{Q}/\dot{m} = (\dot{m}_f/\dot{m})h_c \tag{7}$$

where $\dot{m}$ is the mass flow rate of the fuel/air mixture at a given axial location, and h_c is the heat of combustion per unit mass of fuel. If the variation of cross-sectional area is ignored, the linearized mass flow-rate fluctuation and basic acoustic relations lead to [16]

$$\frac{\dot{m}'}{\bar{\dot{m}}} = \frac{(\rho u)'}{\bar{\rho}\,\bar{u}} = \frac{\rho'}{\bar{\rho}} + \frac{u'}{\bar{u}} = \frac{1}{\gamma}\frac{p'}{\bar{p}} - \frac{p'/(\bar{\rho}\,\bar{a})}{\bar{M}\,\bar{a}} = \left(1-\frac{1}{\bar{M}}\right)\frac{1}{\gamma}\frac{p'}{\bar{p}} \tag{8}$$

Thus, the fluctuating heat release can be related to the acoustic oscillation as

$$\begin{aligned}\frac{q'}{q}\bigg|_{x_f,t} &= \frac{\dot{m}_f'}{\bar{\dot{m}}_f}\bigg|_{x_f,t} - \frac{\dot{m}'}{\bar{\dot{m}}}\bigg|_{x_f,t} = -\frac{\dot{m}'}{\bar{\dot{m}}}\bigg|_{x_i,t-\tau_c} \\ &= \left(\frac{1}{\bar{M}}-1\right)\frac{1}{\bar{\gamma}}\frac{p'}{\bar{p}}\bigg|_{x_i,t-\tau_c} = \left(\frac{1}{\bar{M}}-1\right)\frac{1}{\gamma}\frac{p'}{\bar{p}}\bigg|_{x_f,t-\tau_c-\tau_a}\end{aligned} \tag{9}$$

where x_i is the location of the fuel injector, τ_a is the time for the acoustic wave propagating from the flame zone to the injector, and τ_c is the time for the fluctuating mixture convected from the fuel injector to the flame zone. Note that the fuel injection rate is assumed to be fixed in the above formulation. These two time scales are determined by the local acoustic and convective velocities as follows:

$$\tau_a = \int_{x_i}^{x_f}\frac{\mathrm{d}x}{a-u} \approx \frac{L_{if}}{\underline{a}-\underline{u}} \tag{10}$$

$$\tau_c = \int_{x_i}^{x_f}\frac{\mathrm{d}x}{u} \approx \frac{L_{if}}{\underline{u}} \tag{11}$$

The characteristic frequency for the acoustic-convective feedback loop between the fuel injector and flame zone is

$$f_{if} = 1/\tau_{if} = 1/(\tau_a+\tau_c) \approx \left[\frac{L_{if}}{\underline{a}\,\underline{M}(1-\underline{M})}\right]^{-1} \tag{12}$$

At this characteristic frequency, the Rayleigh's criterion [17] for instability is satisfied, that is, the heat-release fluctuation q' is in phase with the pressure oscillations p' in the flame zone.

E. Comparison Between Measurements and Analytical Prediction

The above analysis is applied to explain the oscillation frequencies observed for the testing conditions in Fig. 7. The characteristic oscillation frequencies, f_{sf1}, f_{sf2}, and f_{if}, are calculated from Eqs. (6) and (12) for each condition. The length scales of these feedback mechanisms, L_{sf} and L_{if}, are determined from the relative distances from the flame location (x_f) to the injection site (x_i) and precombustion shock (x_s), respectively. The shock location is defined as the position where the pressure tap inside the isolator

Table 2 Measured and predicted frequencies of pressure oscillation in scramjet combustor

Case	Run	Inj.	ER	$\mathrm{ER_{body}}$	x_i, cm	x_f, cm	x_s, cm	L_{sf}	L_{if}	T, K	M	f_{sf1}, Hz	f_{sf2}, Hz	f_{if}, Hz		$f_{\exp}$, Hz	
1	F06305AP	I2	0.60	0.60	81.79	101.8	55.8	46.0	20.0	900	0.85	181	167	383	368	496	——
2	F06305AS	I2/I3	0.62	0.37	79.25	99.5	48.2	51.3	20.2	900	0.85	163	149	379	120	——	——
3	F06305AU	I2/I4	0.62	0.37	81.79	102.1	43.1	59.0	20.3	900	0.85	141	130	377	136	168	——
4	F06305AQ	I2	0.81	0.81	81.79	102.2	38.1	64.1	20.4	900	0.85	130	120	376	368	——	——
5	F06305AR	I2/I3	0.80	0.48	79.25	99.9	25.4	74.5	20.6	900	0.85	112	103	371	176	260	292
6	F06305AT	I2/I4	0.84	0.50	81.79	102.4	22.8	79.6	20.6	900	0.85	105	96	372	276	——	——
7	F06305AO	I1	0.64	0.64	76.71	96.7	43.1	53.6	20.0	900	0.85	156	143	384	376	——	——
8	F06305AM	I1/I3	0.64	0.38	76.71	97.0	35.5	61.5	20.3	900	0.85	136	125	378	120	132	252
9	F06305AL	I1/I4	0.64	0.38	79.25	100.0	38.1	61.9	20.7	900	0.85	135	124	369	144	——	——
10	F06305AJ	I1	0.81	0.81	76.71	97.8	12.7	85.1	21.1	900	0.85	98	90	364	316	336	——
11	F06305AN	I1/I3	0.84	0.50	76.71	97.9	7.62	90.3	21.2	900	0.85	92	85	362	244	——	——

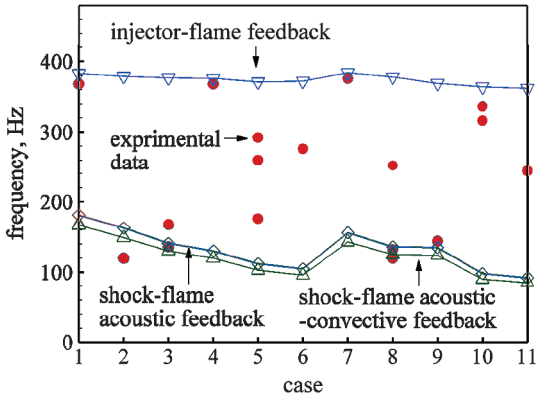

Fig. 9 Flow oscillation frequencies obtained from experimental measurements and analytical predictions based on various feedback loops.

detects the initial pressure rise due to the presence of a shock train. The flame location cannot be easily identified since the combustion spans an extended region starting from the cavity leading edge, as shown in Fig. 4. For simplicity and consistency, in the present study, the flame location is taken as a representative point where the flow is choked (downstream of the peak pressure location). Acoustic perturbation beyond this point cannot propagate upstream through the freestream, except in such subsonic regions as wall boundary layers, whose significance is ignored herein due to their secondary effect. The present study ignores the significance of the wall boundary layer and corner flows in transmitting upstream-traveling acoustic perturbations from the regions downstream of the choked point.

The remaining parameters to be identified are the longitudinally averaged Mach number M and the speed of sound a in Eqs. (4), (5), and (12). Both parameters can be reasonably estimated using the numerical analysis described in [7]. An average temperature of 900 K, along with the typical specific heat ratio and gas constant, were employed to obtain the speed of sound of 601 m/s in the feedback zones. The corresponding average Mach number was about 0.85.

Table 2 lists the experimentally measured and analytically predicted oscillation frequencies. They are also summarized in Fig. 9. There can be more than one dominant oscillation frequencies identified for certain test conditions, as can be seen in Fig. 7. Nearly all the measured oscillation frequencies fall in the range stipulated by the shock–flame acoustic-convective and the injector–flame feedback loops, f_{sf2} and f_{if}, respectively. The two shock–flame feedback frequencies, f_{sf1} and f_{sf2}, are quite close to each other, mainly due to the high subsonic-flow Mach number in that region. Both the shock–flame and injector–flame instability mechanisms were observed in most experiments, and the corresponding frequencies match the predictions reasonably well. It should be noted that, however, due to the several simplifications adopted in the analytical model, the predicted frequencies may have moderate uncertainties. For example, a 2% error in flame location might lead to about 5–10% error in frequencies. Further comparisons show that the feedback loop between the combustion zone and the body-side injection site is responsible for the flow oscillation observed during fueling from the body wall only. For the fueling scheme with 60/40 fuel split between the body and cowl walls (for example, I2/I3), the feedback loop between the combustion zone and the precombustion shock is responsible for the observed flow oscillation.

IV. Conclusions

The thermoacoustic instabilities inside an ethylene-fueled scramjet combustor with a recessed-cavity flameholder were investigated both experimentally and analytically. Flow oscillations with frequencies of 100–400 Hz inside the engine flowpath were measured and the underlying mechanisms were identified. The observed phenomena result from the interactions between the unsteady combustion in the flame zone and the transient responses in the precombustion shock and fuel mixing, respectively. The shock–flame feedback loop dictates the lower bound of oscillation frequencies, whereas the injector–flame loop predicts the upper bound. The effects of fuel/air equivalence ratio, fueling scheme, and simulated flight conditions on the oscillation characteristics were studied systematically. As the equivalence ratio increases, the low-frequency pressure oscillation becomes weaker, indicating a shifting of the driving mechanism from the shock–flame to the injector–flame loop. A similar trend was found when the fueling scheme is switched from a 60/40 fuel split between the body- and cowl-side injection to 100% body-side injection.

Acknowledgments

This work was sponsored by the U.S. Air Force Research Laboratory (AFRL), Propulsion Directorate, under contract number F33615-03-D-2326 (Contract Monitor: Robert Behdadnia). Assistance from the air facility group of the AFRL is acknowledged. The authors would also like to thank Paul Kennedy (AFRL, Propulsion Directorate, Aerospace Propulsion Division), Matthew Streby and Steven Enneking (Taitech, Inc.) for their great assistance in rig operation, data acquisition, and hardware design and setup.

References

[1] Culick, F. E. C., and Yang, V., "Prediction of the Stability of Unsteady Motions in Solid Propellant Rocket Motors," *Nonsteady Burning and Combustion Stability of Solid Propellants*, edited by L. DeLuca, and M. Summerfield, Vol. 143, Progress in Astronautics and Aeronautics, AIAA, Washington, D.C., 1992, pp. 719–779.

[2] Yang, V., and Anderson, W. E. (eds.), *Liquid Rocket Engine Combustion Instability*, Vol. 169, Progress in Astronautics and Aeronautics, AIAA, Washington, D.C., 1995.

[3] Dranovsky, M., and Yang, V., *Combustion Instabilities in Liquid Rocket Engines: Testing and Development Practices in Russia*, edited by F. E. C. Culick, and D. G. Talley, Vol. 221, Progress in Astronautics and Aeronautics, AIAA, Washington, D.C., 2007.

[4] Lieuwen, T. C., and Yang, V. (eds.), *Combustion Instabilities in Gas Turbine Engines: Operational Experience, Fundamental Mechanisms, and Modeling*, Vol. 210, Progress in Astronautics and Aeronautics, AIAA, Washington, D.C., 2005.

[5] Crump, J. E., Schadow, K. C., Culick, F. E. C., and Yang, V., "Longitudinal Combustion Instabilities in Ramjet Engines: Identification of Acoustic Modes," *Journal of Propulsion and Power*, Vol. 2, 1986, pp. 105–109. doi:10.2514/3.22852

[6] Choi, J. Y., Ma, F. H., and Yang, V., "Combustion Oscillations in a Scramjet Engine Combustor with Transverse Fuel Injection," *Proceedings of the Combustion Institute*, Vol. 30, No. 2, 2005, pp. 2851–2858. doi:10.1016/j.proci.2004.08.250

[7] Ma, F. H., Li, J., Yang, V., Lin, K. C., and Jackson, T. A., "Thermoacoustic Flow Instability in a Scramjet Combustor," AIAA Paper 2005-3824, July 2005.

[8] Fry, R. S., "A Century of Ramjet Propulsion Technology Evolution," *Journal of Propulsion and Power*, Vol. 20, No. 1, 2004, pp. 27–58. doi:10.2514/1.9178

[9] Baurle, R. A., and Eklund, D. R., "Analysis of Dual-Mode Hydrocarbon Scramjet Operation at Mach 4-6.5," *Journal of Propulsion and Power*, Vol. 18, No. 5, 2002, pp. 990–1002. doi:10.2514/2.6047

[10] Mathur, T., Gruber, M. R., Jackson, K., Donbar, J., Donaldson, W., Jackson, T., and Billig, F., "Supersonic Combustion Experiments with a Cavity-Based Fuel Injector," *Journal of Propulsion and Power*, Vol. 17, No. 6, 2001, pp. 1305–1312. doi:10.2514/2.5879

[11] Li, J., Ma, F. H., Yang, V., Lin, K. C., and Jackson, T. A., "A Comprehensive Study of Ignition Transient in an Ethylene-Fueled Scramjet Combustor," AIAA Paper 2007-5025, July 2007.

[12] Culick, F. E. C., and Rogers, T., "The Response of Normal Shocks in Diffusers," *AIAA Journal*, Vol. 21, No. 10, 1983, pp. 1382–1390. doi:10.2514/3.60147

[13] Yang, V., and Culick, F. E. C., "Analysis of Unsteady Inviscid Diffuser Flow with a Shock Wave," *Journal of Propulsion and Power*, Vol. 1, No. 3, 1985, pp. 222–228. doi:10.2514/3.22784

[14] Oh, J. Y., Ma, F. H., Hsieh, S. Y., and Yang, V., "Interactions Between Shock and Acoustic Waves in a Supersonic Inlet Diffuser," *Journal of Propulsion and Power*, Vol. 21, No. 3, 2005, pp. 486–495. doi:10.2514/1.9671

[15] Wong, H. Y. W., "Overview of Flow Oscillations in Transonic and Supersonic Nozzles," *Journal of Propulsion and Power*, Vol. 22, 2006, pp. 705–720. doi:10.2514/1.12723

[16] You, D. N., Huang, Y., and Yang, V., "A Generalized Model of Acoustic Response of Turbulent Premixed Flame and Its Application to Gas-Turbine Combustion Instability Analysis," *Combustion Science and Technology*, Vol. 177, 2005, pp. 1109–1150. doi:10.1080/00102200590927012

[17] Culick, F. E. C., "A Note on Rayleigh's Criterion," *Combustion Science and Technology*, Vol. 56, 1987, pp. 159–166. doi:10.1080/00102208708947087

C. Segal
Associate Editor